18th International Conference on Information Fusion
Washington, DC - July 6-9, 2015

# Joint Radar Alignment and Odometry Calibration

Dominik Kellner, Michael Barjenbruch
and Klaus Dietmayer
Institute of Measurement, Control and Microtechnology
Ulm University, Germany
Email: firstname.lastname@uni-ulm.de

Jens Klappstein
and Juergen Dickmann
Environmental Perception
Daimler AG, Germany
Email: firstname.lastname@daimler.com

***Abstract*—An unsupervised online procedure for the precise alignment of fully integrated Doppler radar sensors is proposed. Alignment is the precise determination of the angle between the principal beam direction of the radar sensor and the thrust axis of the vehicle. The method is based on the accurate determination of the sensor movement through the analysis of the Doppler distribution of stationary targets over the azimuth angle. The precise alignment facilitates estimating the ego motion of the vehicle. The approach is long-term stable and bias free and therefore predestined for the calibration of standard vehicle's odometry (gyroscope and wheel sensors). A hierarchical optimization strategy to obtain the systematic errors is presented and Maximum Likelihood estimators are derived for each step. A Monte-Carlo simulation is used to identify critical impact factors and determine them quantitatively. The performance of all approaches is finally evaluated with promising results using measurements obtained by a pre-series 77 GHz Doppler radar sensor. An alignment precision on the order of 0.01-0.05° is achieved.**

## I. Introduction

For Advanced Driver Assistance Systems (ADAS), two main challenges are the sensor-based environmental perception and the ego vehicle's state estimation (position and motion state). Their accuracy strongly depends on a number of extrinsic (sensor mounting position and alignment) and intrinsic parameters of different odometry sensors such as gyroscopes or wheel-based odometry (bias and scaling error).

An error in the sensor alignment is potentially one of the most significant problems in radar systems [1]. For example, an alignment error of 1° induces a lateral offset of 1.75 m of observed objects in a distance of 100 m. An offset of this magnitude invariably leads to fails when associating traffic participants to road lanes. In order to generate an occupancy map of the static environment, the sensor orientation must be known precisely. Otherwise the occupancy map will be blurred and e.g. the estimation of free-space imprecise.

An error in the standard vehicle's odometry additionally deteriorates the mapping errors. Further, the tracking of moving objects (e.g. other traffic participants) requires a precise compensation of the ego vehicle motion by the odometry. Otherwise an erroneous velocity or yaw rate is injected in the motion states of tracked objects and only an unreliable determination of their trajectories and collision risks becomes possible. A precise estimation of the ego vehicle's state is essential not only for the stability control, but for a precise localization as well, e.g. for autonomous driving when the GPS signal is poor.

Radar motion (RM) is an approach to determine the sensor and vehicle's ego-motion in a single measurement cycle [2]. It classifies stationary targets and simultaneously analyzes their Doppler velocity distribution over the azimuth angle. Besides the precise estimation of the ego motion, a crucial property of the approach is a stable long-term accuracy. Because it lacks systematic errors and drift over time, the approach is well suited as the reference system for an unsupervised calibration of the sensor alignment and an online calibration of standard vehicle's odometry systems. The structure of this paper is as follows:

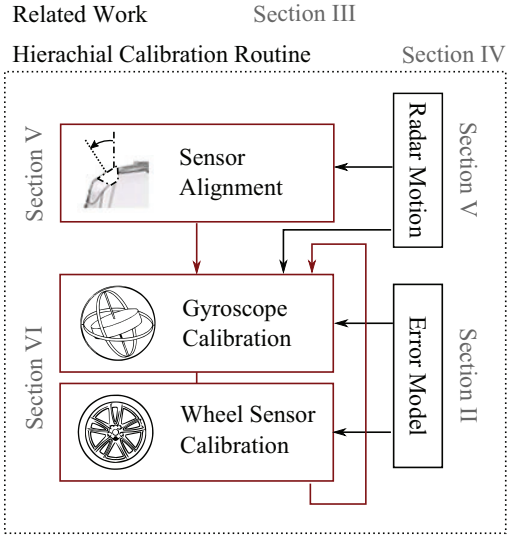


## II. Error modeling

Errors can be classified as either systematic or non-systematic. Non-systematic errors occur randomly and contain non-ascertainable incidents such as wheel slippage and measurement uncertainty. The latter is assumed to have a normal distribution $\mathcal{N}\left(0, \sigma^2\right)$ with zero-mean and standard deviation $\sigma$. Systematic errors are deterministic, sensor specific and usually do not change over a short period of time. All errors are discussed in the following section according to [3]–[5] and critical parameters are identified.

### A. Wheel sensors

Combining the measured rotation rate of all four wheels allows the velocity of the vehicle $v_W$ (true value: $\tilde{v}_v$) at the center of the rear axis to be determined. The systematic errors of wheel sensors arise due to a variation in wheel radius caused by wear on the tires, variations in tire pressure or vehicle load. Furthermore, there is an uncertainty about the effective wheel base, due to no-point contact of wheel-surface. Non-systematic errors occur due to wheel slippage and a dynamic interaction with the road (e.g. bumps, potholes). The rotation rate of the wheels is multiplied by its radius to obtain the velocity. The effects discussed above directly result in a scaling error $\alpha_W$. There is no bias error present.

$$v_W = \alpha_W \cdot \tilde{v}_v + \mathcal{N}\left(0, \sigma_W^2\right) \tag{1}$$

### B. Gyroscope

The errors are discussed for an inexpensive MEMS-gyroscope, which is widely used in the automotive domain. It determines the yaw rate of the vehicle $\omega_G$ (true value: $\tilde{\omega}$). The systematic error is mainly a bias errors $\delta_G$. One component is a warm-up bias which is present for several minutes after the gyroscope is switched on until a constant temperature is reached. The random bias, also called run-to-run drift, is always present during operation. A scale factor error $\alpha_G$ also exists.

$$\omega_G = \alpha_G \cdot \tilde{\omega} + \delta_G + \mathcal{N}\left(0, \sigma_G^2\right) \tag{2}$$

## III. Related Work

This paper addresses the problem of calibrating odometry and exteroceptive sensors at the same time. This problem is widely studied in the field of robotics, relating to a variety of sensor setups and algorithms. The problem is a chicken-and-egg problem. The methods for the sensor pose calibration assume that the odometry is already calibrated, whereas the calibration of the odometry can only be performed with a calibrated exteroceptive sensor [6].

The reference systems used are primarily global positioning systems such as GPS or exteroceptive sensors such as cameras [7] or laser scanners [8]. In the literature, there is no existing system which uses integrated and existing ADAS radar sensors as the reference system.

### A. Sensor Alignment

In this section, online calibration methods are considered, running unsupervised during the lifecycle of the radar system. No external test equipment (laser scanners, calibration targets) are required. The approach in [9] estimates the alignment when approaching to a stationary target (e.g. vehicle) in front. The trajectory of the ego vehicle is matched with the measured positions over time of the stationary target. The estimated orientation offset between both curves is the mounting angle. The accuracy of the approach is stated within +/- 0.25°. There must be confidence that the target is stationary, otherwise a systematic error is injected.

A system with three additional antenna elements, which radiate onto the ground in front of the vehicle at 45° from the horizontal plane, is proposed in [10]. By calculating the difference in the Doppler velocity the radar alignment can be specified. However a systematic error is induced if the vehicle is not driving exactly straight or the angle of incidence differs slightly between the radar beams.

### B. Gyroscope & Wheel Sensor Calibration

The first groups of online odometry calibration approaches are probabilistic techniques, which estimate both the pose of the robot and odometry parameters at the same time. A good overview is presented in [6]. Measurement data and prior knowledge about the system and measuring devices are combined in such a way that the error is statistically minimized. The most common techniques are based on a Kalman Filter (KM). The sensor parameters can be directly included in the state vector of the KM. There are two main approaches, the direct and indirect KM. In the direct formulation the filter acts as an observer, it combines all available sensors and its output is a probabilistic position of the vehicle. In the indirect formulation, a primary set of sensors obtain the state of the vehicle directly. The aim of the KM is to calculate a correction term by comparing the primary set of sensors with an external data source to compensate systematic errors [11]. For the extended Kalman Filter the problem of linearization and outlier suppression is still challenging [6].

However in case of nonlinear systems, smoothing techniques based on iterative optimization are usually superior in terms of accuracy [12]. Using a laser range finder for an indoor environment [8] phrases the problem as a maximum likelihood estimation problem. In comparison, [13] directly estimates the physical parameters of the robot (like wheel radii) through the formulation of a joint estimation problem for localization, mapping and odometry parameters. A laser scanner and wheel encoders are used to determine the state parameters on the fly (sensor positions and odometry calibration). Using structure from motion, [7] performs an auto-calibration of the intrinsic camera parameters. The visual information of the calibrated camera is then fused with inertial sensors to perform real-time navigation.

## IV. System Overview

### A. Problem Formulation

Although the vehicle is factory-calibrated, the parameters such as sensor alignment or wheel radius change over time due to vibration and thermal expansion. A continuous calibration is necessary to deal with time-varying parameters. The parameters have to be inferred from noisy data, e.g. the radar sensor alignment cannot be measured highly accurate directly. The systematic errors of gyroscopes and wheel-speed sensors can only be estimated by a comparison of their noisy data to a noisy reference system.

The approach has to process random trajectories and motion states, since no special calibration trajectories should be carried out by the driver. Therefore not all parameters are always

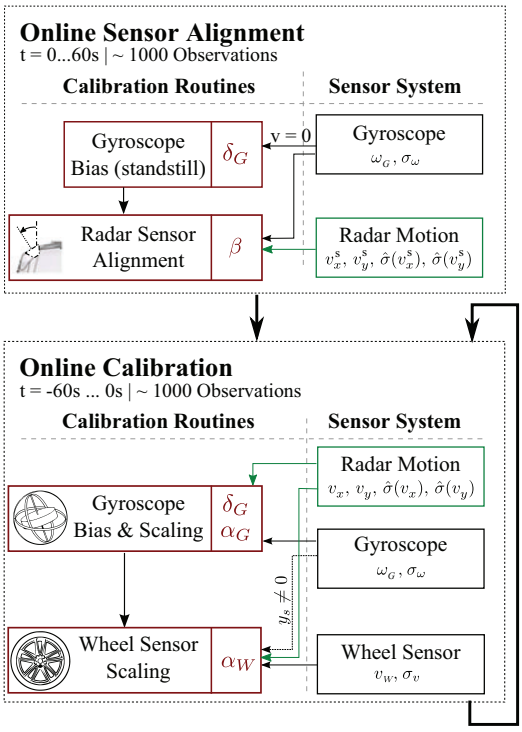


Fig. 1. Overview of the system procedure with initial sensor alignment and calibration of the gyroscope and wheel sensors

observable, e.g. the scaling factor of a gyroscope cannot be estimated on a straight road. Furthermore, temporarily unobservable parameters may appear observable in the presence of noise. Even on a straight road, non-zero yaw rates are measured due to sensor noise. If the measurements are not independent, but anyhow correlated to the noisy measurements of the reference system, a false scaling factor of the gyroscope is observed.

A Kalman Filter is not the best choice for two reasons. First the algorithm has to deal with outliers due to non-systematic errors in odometry (e.g. wheel slip), but as well in radar motion. The second reason is the unobservability, which cannot be directly detected and compensated in a Kalman Filter.

### B. System Procedure

To address the issues of the previous sections, the algorithm listens to an incoming stream of sensor measurements and automatically accumulates the last $N$ of them (further called observations). The algorithm is applied on these observations and determines the sensor parameters as well as a corresponding confidence. A following algorithm (not part of this paper) updates the estimated parameters according to these confidences.

A hierarchically organized algorithm is applied to the calibration problem to overcome the chicken-and-egg problem. Three different error models are employed, according to the state of the sensor. The complete system procedure is shown in Fig. 1. An initial guess for the calibration parameters is not required.

The initial calibration starts after the warm-up period of the gyroscope is finished and the vehicle has stood still for a certain time. The ideal output of the gyroscope is zero while standing still. A scaling error has no effect. By calculating the mean value of the yaw rate while standing still, the current bias $\delta_G$ is estimated. Afterwards it can be assumed that a bias free yaw rate is provided for several minutes. To suppress errors caused by a lateral drift at the rear axle, only measurements with a yaw rate smaller than a threshold are taken into account in the following steps. With this assumption the sensor alignment can be determined by comparing the sensor motion obtained by RM with the gyroscope.

With a precise sensor alignment, RM provides a bias free estimation of the motion parameters of the vehicle. In an online calibration, the bias and scaling factor of the gyroscope and of the wheel sensors can be estimated continuously. They can be determined more accurately with a larger number of observations taken into account, but the reference point is postponed at an earlier point in time. The gyroscope can be readjusted independently of the wheel sensor. If the sensor is not laterally centered the wheel sensor readjustment needs a yaw rate estimation, obtained by either gyroscope or RM.

## V. Radar Alignment

Radar Motion determines the velocity vector of the radar in the sensor coordinate system. When the vehicle moves linearly ($\omega = 0$), this vector has to be parallel to the trust axis of the vehicle. The deviation of the estimated velocity direction corresponds to the mounting orientation (alignment). Since a complete linear movement is rarely present, the idea is extended in this section to random trajectories ($\omega \neq 0$).

### A. Radar Motion - Sensor Motion Estimation

Radar Motion requires no prior knowledge of the environment and can be deployed self-contained on any Doppler Radar sensor. The only input needed is the exact mounting position of the sensor, taken e.g. from CAD data.

If a radar sensor is moved, from its point of view all stationary targets $i = 1...M$ move in the opposite direction. Their relative velocity is exactly inverse to the sensor's velocity vector $\boldsymbol{v^S}$ (heading direction $\gamma^S$). However, it is not possible to directly extract the velocity vectors of the targets as a Doppler radar can only measure the radial velocity component $v_i^D$ under the corresponding azimuth position $\theta_i^S$. For that reason, it is necessary to reconstruct the sensor's velocity vector out of at least two received stationary targets as illustrated in Fig. 2 - left. But to improve the accuracy it makes sense to include all detected stationary targets and determine the movement with a regression calculation. The key point is to examine the sinusoidal progress of the measured radial velocities over the azimuth angle, further called velocity profile.

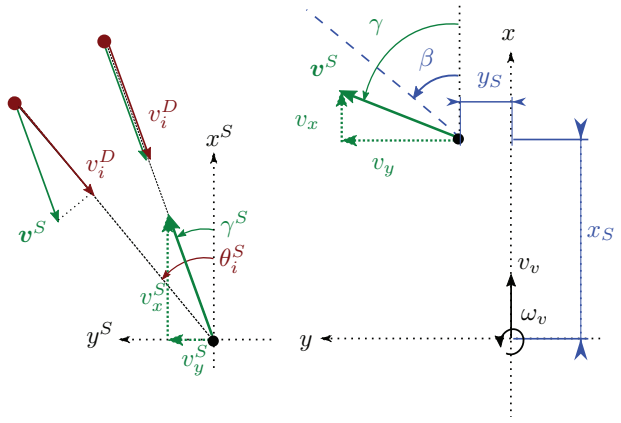


Fig. 2. System parameters in sensor (left) and vehicle (right) coordinate system, with stationary radar targets (red) and radar sensor (black)

An Orthogonal-Distance Regression (ODR), described in detail in [14] (Section III-D), is used to calculate the velocity profile based on the linear equation system of all stationary targets:

$$\begin{bmatrix} -v_1^D \\ \vdots \\ -v_M^D \end{bmatrix} = \begin{bmatrix} \cos(\theta_1^S) & \sin(\theta_1^S) \\ \vdots & \vdots \\ \cos(\theta_M^S) & \sin(\theta_M^S) \end{bmatrix} \begin{bmatrix} v_x^S \\ v_y^S \end{bmatrix} \tag{3}$$

$$-\mathbf{v^D} = \mathbf{M}\ \mathbf{v^S}$$

To identify the stationary targets a RANdom SAmple Consensus (RANSAC) [15] is used, assuming that the largest group of targets with the identical velocity vector forms the stationary targets. Along with the instantaneous estimation of the motion parameters, their corresponding confidence values are estimated. The covariance of a linear equation system (3) is approximated using its inverse Hessian Matrix and the reference variance of all targets [16]:

$$\mathrm{Cov}(\mathbf{v^S}) = \begin{bmatrix} \hat{\sigma}(v_x^S)^2 & \mathrm{Cov}_{xy} \\ \mathrm{Cov}_{xy} & \hat{\sigma}(v_y^S)^2 \end{bmatrix} = \frac{(\epsilon^T \epsilon)(\mathbf{M^T M})^{-1}}{N-2} \tag{4}$$

$$\text{with: } \epsilon = \mathbf{M}\ \mathbf{v^S} - \mathbf{v^D}$$

The corresponding model for the estimates of RM is:

$$\begin{bmatrix} v_x^S \\ v_y^S \end{bmatrix} = \begin{bmatrix} \tilde{v}_x^S \\ \tilde{v}_y^S \end{bmatrix} + \mathcal{N}\left(\mathbf{0}, \mathrm{Cov}(\boldsymbol{v^S})\right) \tag{5}$$

Outliers can occur e.g., when the sensor is obscured and the velocity profile of moving objects is misinterpreted. In this case a good confidence value is returned by RM and the calibration routine has to identify this outlier.

### B. Initial Calibration - Radar Alignment

The alignment of the radar sensor $\beta$ (Fig. 2) is estimated by comparing the lateral velocity at the sensor position determined by the gyroscope ($v_y$) and by RM ($v_y^S$). At each time step $i$, both velocity estimations should be equal

$$|\boldsymbol{v}^S| \cdot \sin\left(\gamma_i^S + \beta\right) = \alpha_G \cdot \omega_{G,i} \cdot x_S \tag{6}$$

so that $\beta$ can be determined by:

$$\beta = \arcsin\left(\alpha_G \cdot \chi_i\right) - \gamma_i^S \tag{7}$$

with the argument $\chi_i = \frac{\alpha_G \cdot x_S}{|\boldsymbol{v}^S|}$. By determining the average alignment over multiple observations, an error due to a gyroscope scaling error ($\alpha_G \neq 1$) is only present if the average value $\mu(\chi) = \frac{1}{N}\sum_{i=1}^{N}\chi_i$ is not equal to zero. In this case a bias is injected in the alignment estimation.

Alternatively, one can estimate the alignment and the scaling error $\alpha_G$ simultaneously (2 DOF). Using a Taylor-Approximation, (7) can be rewritten as a linear equation system with the unknown parameters $\alpha_G$ and $\beta$:

$$\gamma_i^S = \alpha_G \cdot \arcsin(\chi_i) - \beta_i \tag{8}$$

The error caused by the Taylor-Approximation is relatively small for a small $\chi_i$:

$$\epsilon\left(\beta_i\right) \approx \frac{{\alpha_G}^3 - \alpha_G}{6}\chi_i^3 \tag{9}$$

To limit the maximum error of this approximation to 0.1% for a single measurement with a postulated scaling error of maximal 1%, all measurements with a $\chi_i$-value larger than 0.49 have to be excluded. This is equivalent to a yaw rate of 140 °/s, for a vehicle driving at 5 m/s. This restriction increases linearly with larger velocities. Since the yaw rate is restricted anyway due to a potential lateral drift to smaller values (< 30 °/s), the influence of the approximation is negligible.

For the maximum likelihood estimation (Sec. VII) the standard deviation of the current estimation of $\beta_i$ is required. Since the equations are non-linear, a Taylor approximation neglecting correlations is used for error propagation [17]. First the standard deviation of $\gamma^S = \arctan(v_y^S / v_x^S)$ is calculated:

$$\hat{\sigma}_i(\gamma_i^S) = \frac{\sqrt{\left(v_{x,i}^S \cdot \hat{\sigma}_i(v_y^S)\right)^2 + \left(v_{y,i}^S \cdot \hat{\sigma}_i(v_x^S)\right)^2}}{(|\boldsymbol{v}^S|)^2} \tag{10}$$

and of $\chi_i$:

$$\hat{\sigma}_i\left(\chi_i\right) = x_s \sqrt{\frac{\sigma_\omega^2 + \omega_{G,i}^2 \frac{\left(v_{x,i}^S \cdot \hat{\sigma}_i(v_x^S)\right)^2 + \left(v_{y,i}^S \cdot \hat{\sigma}_i(v_y^S)\right)^2}{(|\boldsymbol{v}^S|)^4}}{(|\boldsymbol{v}^S|)^2}} \tag{11}$$

and for the arcus sine:

$$\hat{\sigma}_i\left(\arcsin\left(\chi_i\right)\right) = \sqrt{\frac{\hat{\sigma}_i\left(\chi_i\right)^2}{1-\chi_i^2}} \tag{12}$$

so that the standard deviation of $\beta_i$ is equal to:

$$\hat{\sigma}_i(\beta_i) = \sqrt{\hat{\sigma}_i\left(\arcsin\left(\chi_i\right)\right)^2 + \hat{\sigma}_i(\gamma_i^S)^2} \tag{13}$$

The accuracy of each estimation not only depends on the accuracy of the velocity profile fit, but on the current motion as well. The standard deviations (10) and (12) decrease with a higher absolute velocity $v_v$ at the sensor position, hence the ego-velocity has a significant influence on the estimation accuracy given by Eq. (13). The influence of the yaw rate is difficult to determine, since it affects the absolute velocity $v_v$ for sensors not placed on the x-axis, shifts the ratio of

the velocity components ($v_x$,$v_y$) and has a direct influence on Eq. (11) and (13).

## VI. Odometry Calibration

With an accurate alignment and the knowledge of the sensor position, e.g. by CAD data, it is possible to estimate the ego-motion of the vehicle. By comparing the estimated motion parameters of the gyroscope and wheels sensors with RM, an accurate calibration is possible.

### A. Ego-Motion Estimation

To estimate the vehicle's ego-motion, the sensor velocity has to be transformed in the coordinate system of the vehicle (Fig. 2 - right) using the mounting position ($x_S, y_S$) and orientation $\beta$ of the sensor. Rotating the sensor coordinate system with the mounting orientation, (3) is transformed to:

$$\begin{bmatrix} -v_1^D \\ \vdots \\ -v_M^D \end{bmatrix} = \begin{bmatrix} \cos(\theta_1) & \sin(\theta_1) \\ \vdots & \vdots \\ \cos(\theta_M) & \sin(\theta_M) \end{bmatrix} \begin{bmatrix} v_x \\ v_y \end{bmatrix} \tag{14}$$

with the adapted azimuth position ($\theta_i = \theta_i^S + \beta$). The covariance matrix can be calculated analogous to (4).

The vehicle's velocity $v_v$ and yaw rate $\omega_v$ can be calculated assuming no lateral drift at the rear axle, which can be ensured by excluding measurements with a high yaw rate ($> 30°/s$):

$$\omega_v = \frac{v_y}{x_S} \tag{15}$$

$$v_v = (v_x - y_S \cdot \omega_v) \tag{16}$$

The velocity estimation of the order of 0.01 to 0.1 m/s is highly precise [2], whereas the yaw rate estimation is with 0.5 to 1°/s only slightly worse than of an automotive gyroscope. The update rate of radar is lower (15 - 20 Hz), but it is long-term stable and bias free. Therefore the combination with wheel sensors and gyroscopes shows a high potential.

### B. Online Calibration - Gyroscope

The yaw rate is compared over the extracted observations with the yaw rate estimated by RM $\omega_v$ using eq. (15):

$$\omega_{v,i} = \alpha_G \cdot \omega_{G,i} + \delta_G \tag{17}$$

with the measurement uncertainty:

$$\hat{\sigma}_i(\omega_v) = \frac{\hat{\sigma}_i(v_y)}{x_s} \tag{18}$$

### C. Online Calibration - Wheel Sensor

For wheel sensors a scaling error has to be estimated and compensated. Therefore the estimated velocity at the rear axle of the wheel speed sensors $v_W$ is compared to a joint radar and gyroscope estimation $v_a$:

$$v_{W,i} = \alpha_W \cdot v_{a,i} \tag{19}$$

with

$$v_{a,i} = v_{x,i} + y_S \cdot \omega_{G,i} \tag{20}$$

| | Calibration Routine | Order (DOF) | Estimators | System Equation | Variance Equation |
|---|---|---|---|---|---|
|  | Mounting Orientation | 1 | wMean | (7) | (13) |
| | | 2 | wTLSS | (8) | (12) & (10) |
| | | 2 | wComb | () | () |
|  | Gyroscope | 2 | wTLSS | (17) | (18) & $\sigma_G$ |
|  | Wheel sensor | 1 | wMean | (19) | (22) |

TABLE I
Overview of the calibration routines with the proposed estimators and corresponding equations

and the corresponding standard deviation, using error propagation:

$$\hat{\sigma}_i\left(v_{a,i}\right) = \sqrt{\hat{\sigma}(v_{x,i})^2 + \left(y_S \cdot \sigma_\omega\right)^2} \tag{21}$$

The uncertainty of the scale factor is:

$$\hat{\sigma}_i\left(\alpha_W\right) = \frac{1}{v_{a,i}^2}\sqrt{\left(v_{a,i} \cdot \sigma_v\right)^2 + \left(v_W \cdot \hat{\sigma}_i\left(v_{a,i}\right)\right)^2} \tag{22}$$

## VII. Estimators

In the last two sections, equation systems with corresponding uncertainties were derived. In this section a set of maximum likelihood (ML) estimators is proposed for each of them (Table I). Since the values estimated by RM are not directly measured, but determined by an estimator itself, their covariance matrix ($\hat{\sigma}_i(v_x), \hat{\sigma}_i(v_y)$) differs at each time step $i$. Therefore all estimators have to deal with heteroscedasticity. The variables obtained by RM are directly compared to the yaw rate resp. wheel sensor, so that the measurements are assumed to be uncorrelated.

### A. Choice of Estimator

It is well known that for the estimation of a single parameter (1 DOF) in case of heteroscedasticity, the ML estimator is a weighted arithmetic mean (wMean) with the inverse variance of each sample as weighting factor. Additionally the weighted sample variance is calculated according to [16].

In addition to the heteroscedasticity, a 2 DOF estimator suffers from measurement errors in the dependent as well as in the independent variables. This is called the *errors in variables* (EIV) problem. In general this problem does not admit an analytic solution [18]. A possibility is the weighted total least-square solution (WTLSS) introduced in [19] for the homoscedastic case using a non-linear Lagrange function approach. A procedure for the heteroscedastic case of the straight-line fit problem, where both the dependent and independent variables can have any non-singular variance-covariance matrix is derived in [20]. The solution is based on a set of non-linear Euler-Lagrange conditions and a quickly converting regression scheme is presented based on the method of Lagrange multipliers. Furthermore an estimation of the sample covariance matrix is proposed. The algorithm proposed in Section 4 in [20] is used for the EIV fitting problems.

### B. Outlier Handling

Line fitting based on ML estimation fails when the data set contains outliers that do not satisfy the assumed statistical noise model. Wheel sensor and RM can contain outliers as discussed in Section II-A respectively Section V-A. A RANSAC algorithm is used in a preprocessing step in all routines to exclude these non-systematic errors. Since a Gaussian distribution is assumed and the standard deviations of all variables are known, the distance threshold can be calculated using the chi squared distribution. To include at least 95% of all inliers for the case of 1 DOF $3.85\,\sigma^2$ and of 2 DOF $5.99\,\sigma^2$ are used as the distance threshold. If the standard deviation is not identical during the extracted observations, its mean value is determined. In this preprocessing step the errors-in-variables problem is ignored due to system speed up.

### C. Combination of Estimators

The accuracy of the estimators depends to a great extent not only on the measurement accuracies, but also on environment parameters of the considered observations. Thus the choice of the estimator cannot always be made in advance, especially to avoid the case of unobservability as discussed in Section IV-A. This is particularly the case for the mounting angle calibration respectively gyroscope scale calibration if the variability of the yaw rate $\sigma(\omega_{\text{ob}})$ in the considered observations is small.

The combination of estimators is a widely studied problem in classification and regression estimation. They can be separated in a combination of estimators, performed on the identical data [21] or on bootstrap samples of the data [22], called bagging predictors. In this paper, bootstrapping is not reasonable, due to the outlier handling (previous section) the estimators are stable and contain none or only a small number of outliers. In this case bagging slightly degrades the performance of a single estimator [22].

The principle of a result-driven regularization (weighting) of all estimators is used in this paper. The weighting function can be derived by estimating the sample variance and bias of each estimator. The problem can be specified as a combination of two estimators of $\delta$ (1 DOF $\hat{\delta}_1$ and 2 DOF $\hat{\delta}_2$ and as vector $\hat{\boldsymbol{\delta}}$) with $\tilde{z}_i = \alpha z_i + \delta$. The estimator with 1 DOF has a bias $m_1$, if $\alpha \neq 1$ and the mean value over the observations is $\mu(z) \neq 0$.

In the following, the weighting factors $\mathbf{g} = [g_1\ g_2]^{\mathrm{T}}$ for an optimal combination of both estimators are calculated based on their input data set $f_i$ and their covariance matrix:

$$\mathbf{\Omega_{i,j}} = E_{i,j}((f_i - \hat{\delta}_i) - (f_j - \hat{\delta}_j)) \tag{23}$$

Using the constraint that the sum of the weighting factors is equal to 1 guarantees that the combined estimator is unbiased if the individual estimators are unbiased [23]. The ML-estimator is achieved with the following weights:

$$\mathbf{g} = \left[\mathbf{\Omega}_{1,2} + \left(\hat{\boldsymbol{\delta}} - \delta\mathbf{u}\right)\left(\hat{\boldsymbol{\delta}} - \delta\mathbf{u}\right)^{\mathrm{T}}\right]^{-1}\mathbf{u} \tag{24}$$

where $\mathbf{u} = [1\ \ 1]^{\mathrm{T}}$.

| | Parameter | Variable | Value |
|---|---|---|---|
| Measurement Uncertainty | Yaw rate | $\sigma_\omega$ | 0.5 [°/s] |
| | Odometry | $\sigma_v$ | 0.2 [m/s] |
| | Radar Velocity | $\sigma(v_r)$ | 0.1 [m/s] |
| | Radar Azimuth | $\sigma(\theta)$ | 1 [°] |
| Observation Parameters | Nr of Observations | $i$ = 1...$N$ | 100 |
| | Nr. of Targets | $M$ | $\mathcal{U}(10, 50)$ |
| | Field of View | $\Delta\theta$ | $\mathcal{U}(-45, 45)$ [°] |
| | Velocity | $v_{\text{ob}}$ | 10 [m/s] |
| | Yaw Rate | $\omega_{\text{ob}}$ | $\mathcal{N}(5, 15)$ [°/s] |
| | Radar Positon | $(x_S, y_S)$ | (3.5, 0) [m] |
| | Radar Orientation | $\beta$ | 0 [°] |

TABLE II
SIMULATION PARAMETERS

## VIII. SIMULATION AND PARAMETER EVALUATION

A Monte-Carlo simulation is performed to analyze the estimators introduced in the previous section for all three stages. The accuracy of RM depends on the number and relation of stationary targets and non-stationary targets and on the Doppler & Azimuth measurement accuracy of the radar sensor, which is analyzed in detail in [2]. This paper investigates the sensor mounting position and the distribution of the velocity $v_{\text{ob}}$ and yaw rate $\omega_{\text{ob}}$ in the considered observations in terms of average $\mu(\cdot)$ and variability $\sigma(\cdot)$.

The simulation is carried out 100.000 times, with the parameters specified in Table II. The standard deviation decreases for all algorithms approximately with the inverse root of the number of observations $\sim 1/\sqrt{N}$. For simulation efficiency, $N$ is set to 100, so that all errors are reduced with a factor of approximately 3 if $N$ is increased to 1000.

### A. Radar Sensor Alignment

The different estimators have a promising accuracy for the estimation of the sensor alignment with a root-mean-squared error (RMSE) below 0.05° (or 0.016° for 1000 observations). The variability of the yaw rate $\sigma(\omega_{\text{ob}})$ in the observations in combination with a gyroscope scaling error $\epsilon(\alpha_G)$ have a major influence on the accuracy of the sensor alignment, as shown in Fig. 3 and Table III. The RMSE of wMean increases only slightly with $\sigma(\omega_{\text{ob}})$, but the bias error increases linearly with an increasing $\epsilon(\alpha_G)$. For wTLSS the RMSE decreases overproportionally with $\sigma(\omega_{\text{ob}})$, whereas a scaling error has no influence. wComb is always more accurate than the best single estimator in terms of the RMSE. wMean has the smallest standard deviation, whereas wTLSS has no bias error.

With a larger average velocity $\mu(v_{\text{ob}})$ the accuracy of the alignment decreases overproportionally $\sim 1/\sqrt{\mu(v_{\text{ob}})}$. There is only a minor influence on the variability of the velocity $\sigma(v_{\text{ob}})$. The sensor alignment $\beta$ itself has only a small influence on the calibration accuracy (+/- 10%).

Further influences are the sensor's mounting position $x_S$. The alignment error decreases roughly with the inverse distance of the sensor to the rear axle $\sim 1/x_S$, whereas the

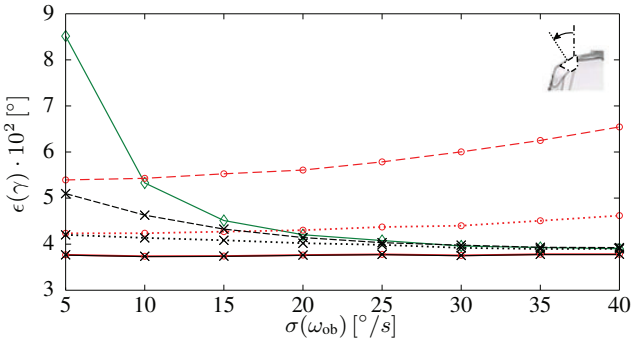


Fig. 3. Accuracy of the sensor alignment $\beta$ in terms of the RMSE for wMean (o - red) and wComb (x - black) for different scaling errors $\epsilon(\alpha_G) = 0$ (—), $\epsilon(\alpha_G) = 0.5\%$ (· · ·) and $\epsilon(\alpha_G) = 1\%$ (- - -). wTLSS (◇ - green) is independent of $\alpha_G$.

| $\epsilon(\alpha_G)$ | Estimators | | |
|---|---|---|---|
| [%] | wMean | wTLSS | wComb |
| 0 | 0.0376 (0.0001) | 0.0480 (0.0001) | 0.0376 (0.0001) |
| 0.5 | 0.0437 (0.0213) | 0.0479 (0.0001) | 0.0402 (0.0102) |
| 1 | 0.0582 (0.0429) | 0.0481 (0.0001) | 0.0426 (0.0109) |
| 2 | 0.0965 (0.0860) | 0.0478 (0.0001) | 0.0451 (0.0192) |

TABLE III
RMSE (BIAS) [°] OF THE RADAR SENSOR ALIGNMENT IN DEPENDENCE OF THE SCALING FACTOR OF THE GYROSCOPE

lateral position $y_S$ does not affect the results. The measurement accuracy of the gyroscope $\sigma_G$ only has a significant influence if the error is of the same magnitude as the yaw rate estimation error of RM. If $\sigma_G$ is increased to 1 °/s the alignment error increases only 15%, whereas if it is doubled from 2 °/s to 4 °/s the orientation error is nearly doubled as well.

### B. Gyroscope Bias and Scaling

For the determination of the gyroscopes' systematic errors only wTLSS is used (Fig. 4), since 2 DOF have to be resolved. The RMSE for the determination of the scaling factor $\alpha_G$ is 1.38 % and the bias $\delta_G$ is 0.22 °/s. Both estimation errors increase linearly with the average velocity $\mu(v_{ob})$. At 20 m/s, the RMSE is 10% or 15% larger, respectively. The reason being that at higher velocity, $\chi$ diminishes, which has the same effect than a smaller variability of the yaw rate $\sigma(\omega_{ob})$.

The estimation of the bias $\delta_G$ is equivalent to the alignment, so that the dependencies are approximately the same as for wTLSS in the previous section. For the estimation of the scale factor $\alpha_G$, the yaw rate variability $\sigma(\omega_{ob})$ has a larger impact. With increasing variability the standard deviation decreases roughly inversely to $\sim 1/\sigma(\omega_{ob})$, whereas the mean value $\mu(\omega_{ob})$ has no influence. The influence of the distance to the rear axle and of the gyroscope measurement accuracy are equivalent to that of the alignment.

### C. Wheel Sensor Scaling

The estimation of a wheel scaling $\alpha_W$ is is relatively small with an RMSE of 0.21%. The two main dependencies

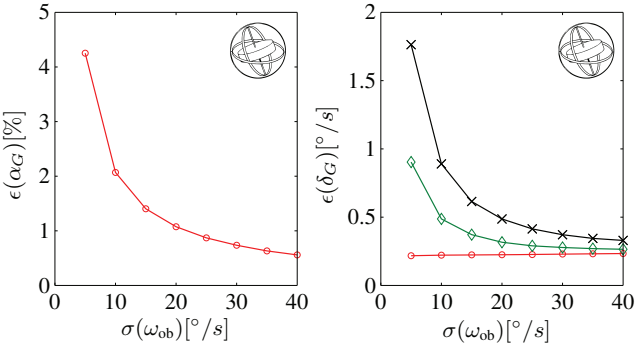


Fig. 4. RMSE for the estimation of the gyroscope scaling factor $\alpha_G$ (left) and bias $\delta_G$ (right) in dependency of the variability of the yaw rate $\sigma(\omega_{ob})$ for different average yaw rates $\mu(\omega_{ob}) = 0\,°/s$ (o - red), $10\,°/s$ (◇ - green) and $20\,°/s$ (x - black)

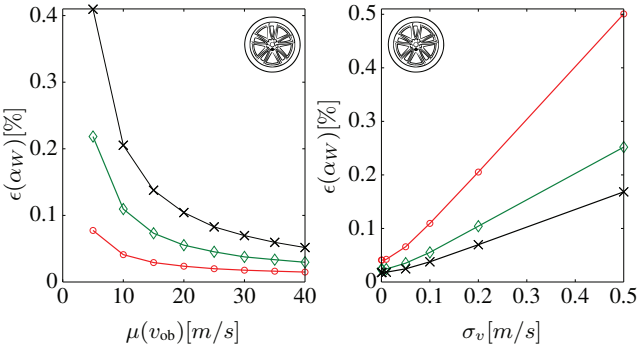


Fig. 5. RMSE for the estimation of the wheel sensor scaling factor $\alpha_W$ dependent on the average velocity of the observations $\mu(v_{ob})$ (left) for different wheel sensor errors $\sigma_v = 0$ (o - red), 0.1 m/s (◇ - green) and 0.2 m/s (x - black) and of the wheel sensor accuracy $\sigma_v$ (right) with an average velocity of $\mu(v_{ob}) = 10$ m/s (o - red), 20 m/s (◇ - green) and 30 m/s (x - black)

are the average velocity of the observations $\mu(v_{ob})$ and the wheel sensor measurement error $\sigma_v$, as can be seen in Fig. 5. The RMSE is almost directly proportional to $\sigma_v$. When $\sigma_v$ is halved (0.1 m/s), the error is decreased from 0.21% to 0.11%. In contrast to the previous parameters, the RMSE decreases with a larger average velocity $\sim 1/\mu(v_{ob})$. The mounting position, yaw rate and the gyroscope measurement error have a negligible influence on the accuracy.

## IX. EXPERIMENTAL RESULTS

The evaluated dataset consists of 12 sequences (2 km each) with low ($\sigma(\omega_{ob}) < 5\,°/s$) and 2 with high ($\sigma(\omega_{ob}) > 8\,°/s$) yaw rate variability, all captured on different days. The average velocity is varied between 5 and 12 m/s, so that 2000 - 4000 measurements are recorded in each sequence and approximately 36000 in total. For the evaluation, a pre-series Doppler radar mounted on the front of the vehicle is used. The azimuth accuracy is up to 4° and the Doppler accuracy 0.04 m/s. Besides the standard vehicle's odometry obtained by the FlexRay bus, a highly precise inertial measurement unit (IMU) with dGPS support is taken as ground truth for the odometry errors.

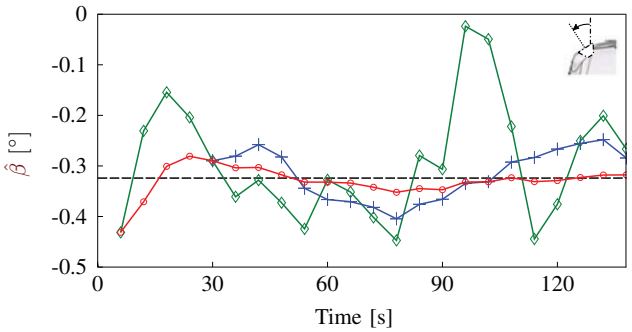


Fig. 6. Estimated sensor alignment $\beta$ for a sample sequence with all available observations (o - red), the last 100 ($\diamond$ - green) and 500 observations (+ - blue) and the estimated orientation over all 12 sequences (- - - - black)

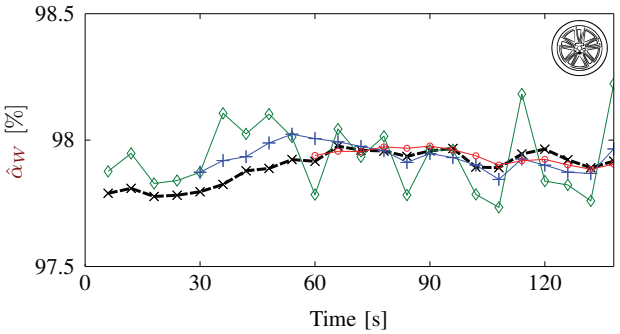


Fig. 7. Estimated wheel sensor scaling factor $\hat{\alpha}_W$ of an example sequence determined by the last 1000 (o - red), the last 500 (+ - blue) and 100 observations ($\diamond$ - green) and by the reference system (x - black)

| | $N = 500$ | $N = 200$ | $N = 100$ | $\hat{\boldsymbol{\beta}}_{\boldsymbol{N},\max}$ |
|---|---|---|---|---|
| $\mu(\hat{\beta})$ | -0.319° | -0.308° | -0.300° | **-0.324°** |
| $\sigma(\hat{\beta})$ | 0.065° | 0.101° | 0.153° | **0.009°** |
| $\max(\hat{\beta}) - \min(\hat{\beta})$ | 0.199° | 0.329° | 0.717° | **0.030°** |

TABLE IV
REPEATABILITY OF THE SENSOR ALIGNMENT ESTIMATION OVER 12 SEQUENCES FOR DIFFERENT OBSERVATION SIZES $N$

| Parameter | Unit | $N = 100$ | $N = 500$ | $\boldsymbol{N = 1000}$ | $N = 1500$ |
|---|---|---|---|---|---|
| $\epsilon(\alpha_W)$ | [%] | 0.113 | 0.059 | **0.040** | 0.022 |
| $\epsilon(\alpha_G)$ | [%] | 2.242 | 1.099 | **0.779** | 0.369 |
| $\epsilon(\delta_G)$ | $[°/s]$ | 0.314 | 0.148 | **0.077** | 0.040 |

TABLE V
RMSE OF THE SYSTEMATIC PARAMETERS OF GYROSCOPE AND WHEELS SENSORS OVER 12 SEQUENCES FOR DIFFERENT OBSERVATION SIZES $N$

### A. Sensor Alignment

To determine the sensor alignment $\beta$ of a system with the same accuracy as the proposed approach ($< 0.05°$) is hardy possible, since the exact angle between the antenna ground plane inside the radar housing and the vehicle's axle has to be measured. Therefore the repeatability over all 12 sequences with varying conditions and different observation sizes is analyzed. A complete sequence is shown in Fig. 6, with a different number of observations $N$ used. If all available measurements are used, the estimation result converges at the end of the sequence.

In Table IV the repeatability is shown over 12 sequences. Firstly the average accuracy over all sequences with three different observation sizes is presented. Secondly the variation between the final alignment estimations $\hat{\beta}_{N,max}$ of all sequences are compared. With a larger observation size the standard deviation of the alignment estimates decrease as expected roughly with $\sim 1/\sqrt{N}$. By comparing the final estimates over the sequences, their standard deviation is a very low 0.009°. Since the estimators are bias free, the result is equal to the RMSE of the approach. The largest difference in between the sequences is a very low 0.03°.

### B. Wheel sensor - Scale error

The second evaluation examines the accuracy of the odometry scaling estimation $\alpha_W$. The ground truth is determined by the last 500 observations. Since no precise measurement of the wheels' diameters, base etc. was made in advance, there is a scaling error $\epsilon(\alpha_W)$ of approx. 2%. As can be seen in Fig. 7, the calibration is able to precisely determine the scaling factor for a sample sequence.

The RSME is shown in Table V over all sequences for different observation sizes. Considering a scaling error which is on the order of 1 - 2%, the error is significantly reduced to a value below 0.05% for observation sizes larger than 600. Further, the error decreases roughly with the inverse root of the section size.

### C. Gyroscope - Bias & Scale Error

The third evaluation analyses the estimation of the gyroscopes' parameters. The scale factor $\alpha_G$ is analyzed on the 2 dynamic sequences with 5000 measurements in total, whereas the bias is analyzed on the 12 non-dynamic sequences. For a single sequence the estimated parameters are shown in Fig. 8 and the errors over all sequences are summarized in Table V.

The accuracy of the scale factor $\alpha_G$ on the order of 0.4 – 2% is relatively large. The gyroscope will have an error approximately on the same order, so that a calibration results in only a small benefit. For non-dynamic scenes, the error increases approximately with a factor of 5 (e.g. for 1000 observations 3.8%). Since wTLSS calculates a covariance matrix, an update of the scaling factor in the final implementation is only performed if the estimated sample variance is significantly smaller than the error of the scale factor specified in the gyroscope datasheet.

The bias error $\delta_G$ of the gyroscope is determined highly precisely with an RMSE of $0.077\,°/s$ for 1000 observations. Even if it is evaluated for only the two dynamic sequences, the error increases only slightly (e.g. $0.118\,°/s$ for 1000 observations).

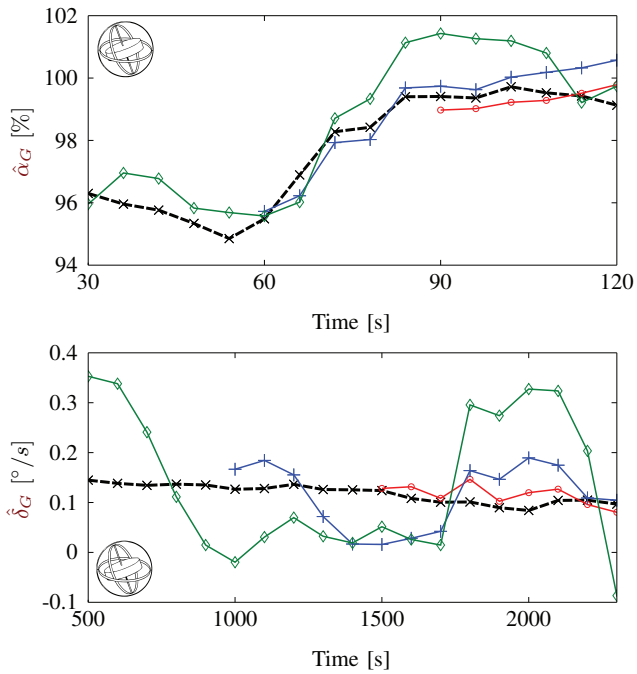


Fig. 8. Estimated gyroscope scaling factor $\alpha_G$ (top) and bias $\delta_G$ (bottom) of an example sequence determined by the last 1500 (o - red), the last 1000 (+ - blue), 500 observations (◇ - green) and ground truth (x - black)

## X. Conclusion

Besides the strategy of the hierarchical calibration procedure, robust maximum likelihood estimators for each subroutine are derived and evaluated on simulated and experimental data. The sensor alignment on the order of 0.01° to 0.05° is more accurate than state of the art methods with 0.25°. The approach can be deployed on any Doppler radar without any modifications. The calibration of standard vehicle's odometry shows promising results. Especially the estimation of the scaling factor of wheel based odometry is highly precise with an RMSE of 0.04%. The determination of the gyroscope bias with an RMSE of 0.07 °/s is also precise. Solely the correction of the scaling factor of the gyroscope is not always practicable with an RMSE of 0.8% and the prerequisite of a trajectory with multiple curves in both directions. However the sample variance of each parameter is estimated simultaneously, so that a correction can be conducted if the parameter is more accurate than the error of the parameter specified in the datasheet of the sensor.

The approach can be extended to multiple radar sensors. After the sensor alignment of each sensor separately, the ego-motion can be determined using all available sensors [14]. Not only will the accuracy be significantly increased, but even arbitrary driving states including lateral drift can be resolved.

## References


[1] R. Abou-Jaoude, "Acc radar sensor technology, test requirements, and test solutions," *Intelligent Transportation Systems, IEEE Transactions on*, vol. 4, no. 3, pp. 115–122, 2003.

[2] D. Kellner, M. Barjenbruch, J. Klappstein, J. Dickmann, and K. Dietmayer, "Instantaneous ego-motion estimation using doppler radar," in *Intelligent Transportation Systems-(ITSC), 2013 16th International IEEE Conference on*. IEEE, 2013, pp. 869–874.

[3] J. Borenstein and L. Feng, "Umbmark: a method for measuring, comparing, and correcting dead-reckoning errors in mobile robots," 1994.

[4] J. Kim, J.-G. Lee, G.-I. Jee, and T.-K. Sung, "Compensation of gyroscope errors and gps/dr integration," in *Position Location and Navigation Symposium, 1996., IEEE 1996*. IEEE, 1996, pp. 464–470.

[5] O. J. Woodman, "An introduction to inertial navigation," *University of Cambridge, Computer Laboratory, Tech. Rep. UCAMCL-TR-696*, vol. 14, p. 15, 2007.

[6] A. Censi, A. Franchi, L. Marchionni, and G. Oriolo, "Simultaneous calibration of odometry and sensor parameters for mobile robots," *Robotics, IEEE Transactions on*, vol. 29, no. 2, pp. 475–492, 2013.

[7] E. Jones, A. Vedaldi, and S. Soatto, "Inertial structure from motion with autocalibration," in *Workshop on Dynamical Vision*, 2007.

[8] N. Roy and S. Thrun, "Online self-calibration for mobile robots," in *Robotics and Automation, 1999. Proceedings. 1999 IEEE International Conference on*, vol. 3. IEEE, 1999, pp. 2292–2297.

[9] U.S. Department of Transportation, "Automotive collision avoidance system field operational test," National Highway Traffic Safety Administration, Tech. Rep., 2003.

[10] M. E. Russell, A. Crain, A. Curran, R. A. Campbell, C. A. Drubin, and W. F. Miccioli, "Millimeter-wave radar sensor for automotive intelligent cruise control (icc)," *Microwave Theory and Techniques, IEEE Transactions on*, vol. 45, no. 12, pp. 2444–2453, 1997.

[11] R. González, F. Rodrıguez, J. Guzmán, and M. Berenguel, "Comparative study of localization techniques for mobile robots based on indirect kalman filter," in *Proceedings of IFR Int. Symposium on Robotics*, 2009, pp. 253–258.

[12] J. Maye, P. Furgale, and R. Siegwart, "Self-supervised calibration for robotic systems," in *Intelligent Vehicles Symposium (IV), 2013 IEEE*. IEEE, 2013, pp. 473–480.

[13] R. Kümmerle, G. Grisetti, and W. Burgard, "Simultaneous parameter calibration, localization, and mapping," *Advanced Robotics*, vol. 26, no. 17, pp. 2021–2041, 2012.

[14] D. Kellner, M. Barjenbruch, J. Klappstein, J. Dickmann, and K. Dietmayer, "Instantaneous ego-motion estimation using multiple doppler radars," in *Robotics and Automation (ICRA), 2014 IEEE International Conference on*. IEEE, 2014, pp. 1592–1597.

[15] M. A. Fischler and R. C. Bolles, "Random sample consensus: a paradigm for model fitting with applications to image analysis and automated cartography," *Communications of the ACM*, vol. 24, no. 6, pp. 381–395, 1981.

[16] C. D. Ghilani, *Adjustment computations: spatial data analysis*. John Wiley & Sons, 2010.

[17] H. Ku, "Notes on the use of propagation of error formulas," *Journal of Research of the National Bureau of Standards*, vol. 70, no. 4, 1966.

[18] N. Kiryati and A. M. Bruckstein, "Heteroscedastic hough transform (htht): An efficient method for robust line fitting in the errors in the variables problem," *Computer Vision and Image Understanding*, vol. 78, no. 1, pp. 69–83, 2000.

[19] B. Schaffrin, I. LEE, Y. CHOI, and Y. FELUS, "Total least-squares (tls) for geodetic straight-line and plane adjustment," *Bollettino di geodesia e scienze affini*, vol. 65, no. 3, pp. 141–168, 2006.

[20] B. Schaffrin and A. Wieser, "On weighted total least-squares adjustment for linear regression," *Journal of Geodesy*, vol. 82, no. 7, pp. 415–421, 2008.

[21] M. P. Perrone, "Improving regression estimation: Averaging methods for variance reduction with extensions to general convex measure optimization," Ph.D. dissertation, Brown University, 1993.

[22] L. Breiman, "Bagging predictors," *Machine learning*, vol. 24, no. 2, pp. 123–140, 1996.

[23] M. Taniguchi and V. Tresp, "Averaging regularized estimators," *Neural Computation*, vol. 9, no. 5, pp. 1163–1178, 1997.